

New 3-5 μ wavelength range hyperspectral imager for ground and airborne use based on a single element interferometer

Dario Cabib*, Amir Gil, Moshe Lavi, Robert A. Buckwald
CI Systems Ltd., Industrial Park Ramat Gavriel, Migdal Haemek, Israel 10551
and
Stephen G. Lipson
Physics Department, Technion-Israel Institute of Technology, Haifa, Israel

ABSTRACT

Spectral imagers rely mainly on two techniques for collection of spectral information: gratings and interferometers. The former type needs cooling of the optics to avoid background signals which significantly limit the dynamic range of the measurement. The latter type, in its present commercial configurations, is not suitable for pushbroom operation in an airborne situation. A recent spectral imager configuration based on a shearing interferometer has been shown to be suitable for pushbroom operation^{1,2} without the need for cooling the optics^{2,3}.

In this paper we describe the planned implementation of such a spectral imager¹ for the 3-5 μ range, where the interferometer is a specially designed single prism. The advantages of this interferometer configuration are: i) compact optics, ii) high S/N ratio in the 3-5 μ range with small optical collection diameter, and iii) enhanced mechanical stability. The instrument yields a spectrum for 320x240 pixels of the image with a spectral resolution of better than 50 cm^{-1} . The spectrum is calibrated in units of $\text{Watt}/(\text{steradian}\cdot\text{cm}^2\cdot\text{cm}^{-1})$. If used in an airborne pushbroom mode it provides a swath width of 240 pixels in a ~ 6.9 degree transverse field of view. If used in a horizon scanning configuration, it has a vertical field of $\sim 6.9^\circ$ and a horizontal field up to 300 degrees. The IFOV is 0.5 milliradians.

In this paper the major instrument design considerations are presented. The instrument is being constructed and we will give more details on actual performance and examples of measurement results in a future paper, as we gain more experience. An 8-12 μ range version is also planned for the near future.

Keywords: Infrared spectral imaging, Hyperspectral imaging, Interferometric imaging

1. INTRODUCTION

During the last decade the field of "Hyperspectral Imaging" or "Imaging Spectrometry", or "Spectral Imaging", as it is called by different people, has grown in leaps and bounds. The number and variety of hyperspectral imagers that have been built and deployed, and the number of papers that have been published in remote sensing conferences and journals about them is enormous. The reader can learn about the existing hardware and applications by referring for example to papers published in the Optical Engineering journal and SPIE conference proceedings^{4,5}. In particular, references 4 and 5 carry an exhaustive list and comparison among the various technologies used for this type of instrumentation over the years. In addition, a large amount of results and knowledge on the capabilities of hyperspectral imaging has been accumulated over those years on both the airborne and space-borne applications: see for example the papers presented at the Remote Sensing SPIE conference held in Gran Canaria on 13-16 September 2004, and the OSA conference held in Alexandria, Virginia on January 31-February 3, 2005, on Hyperspectral Imaging and Sounding of the Environment. For a review of a large number of applications of spectral imaging, see reference 6. For a review of comparison of étendue in different spectral imaging designs, see reference 7.

Pioneering work in Fourier Transform spectral imaging was done at CI Systems in the years 1989-1990: the work established a novel and generic method of collecting and storing hyperspectral imaging data with a design based on an interferometer, combined with collecting optics without slit and a two-dimensional detector array suitable for the visible range. This technology was suitable for staring imaging but not for pushbroom operation. In subsequent years this staring technology, combined with a specially developed multicolor fluorescent DNA hybridization and staining technique, was commercialized by a sister company of CI Systems and was the basis for a breakthrough in the analysis of chromosome abnormalities, published in Science magazine in 1996⁸. Many other publications by a large number of researchers in this field followed in later years.

*dario.cabib@ci-systems.com

It turns out that with a significant modification of the system (described in a later section) this interferometric design can be used in a pushbroom configuration in the visible and infrared ranges, suitable for airborne and space-borne applications. For the instrument to be sensitive in the infrared range the collecting optics and interferometer must be suitable for infrared, and the infrared array is preferably cooled for high signal to noise performance. In this paper we describe this pushbroom modification as implemented in the present work, and the design values of the important performance parameters in the 3-5 μ range. Some expected performance of this design and preliminary test results are also mentioned.

An extensive theoretical modeling paper⁹ of interferometric spectral imaging instruments has been published by Keller and Lomheim in 2005, and we rely on it to predict the sensitivity performance of the present implementation.

2. REVIEW OF THE EARLIER STARING IMAGING TECHNOLOGY

This staring spectral imaging technology is described in detail in reference 10 as implemented in an instrument called SD 200. Figure 1 shows the SD 200 implementation combined with a fluorescence microscope for cancer genetics applications⁸. In this case the system works only in the visible range of the spectrum. The rest of the system of figure 1 is a fluorescence microscope, including special filters for excitation blocking and fluorescence detection.



Figure 1: The SD 200 spectral imager, combined with a fluorescence microscope, being used for very advanced analysis and classification of genetic abnormalities, is not suitable for pushbroom operation.

First the spectral cube of interferograms (one interferogram per pixel) is acquired by rotating the interferometer around an axis parallel to the interferometer mirrors, and by storing in the memory of the computer the different images obtained from the CCD during this rotation. As the interferometer rotates, each pixel of the CCD remains the stationary image of a pixel in the FOV at all times, while the light intensity reaching it is modulated by the resulting optical path difference (OPD) scan. The instantaneous OPD depends on the interferometer position and on the horizontal position of the specific pixel within the Field of View (FOV) of the spectral imager. At the end of the interferometer rotational scan, the signal measured for each pixel as function of OPD is the interferogram corresponding to the spectrum of the pixel as function of wavenumber (or wavelength). In a second step, the interferogram of each pixel is Fourier transformed to obtain the fluorescence spectra of all the pixels of the cube. In a third step, the spectrum of each pixel is analyzed and classified according to a predetermined algorithm or look up table of stored spectra; this information is used to display the image segmented into regions of different colors. Figure 2 shows a more advanced version of the SD 200, as implemented for staring imaging remote sensing in an instrument called SpectraView. It is mounted on a tripod to measure the spectra of every pixel of stationary FOV scenery in the wavelength range 400-1000 nm, and a field lens collects the light instead of the microscope. In the usual case now the illumination is from the environment, particularly sun light, so the cube is a spectral reflectance cube of the object being measured.



Figure 2: The SpectraView spectral imager, equipped with a telescope lens and mounted on a tripod, for remote measurements of objects in the 0.4 to 1 micron spectral range, in a staring configuration (stationary FOV scenery).

Figure 3 shows an example of two frames of the SpectraView, as examples of frames captured by the CCD and seen on the computer screen of the instrument during the interferometer rotation. It is seen that vertical fringes are superimposed on the scenery of the stationary FOV: these fringes are horizontally shifted from one image to the other because the two frames are taken at different interferometer angular positions.

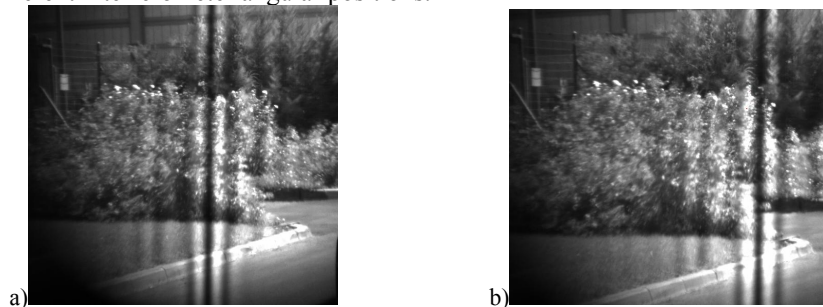


Figure 3: a) FOV frame at a nearly central interferometer position (the central bright fringe is the "zero OPD" fringe); b) the same FOV scene, corresponding to an interferometer off-center angular position: since the interferometer is rotated, the central fringe is not near the central pixel column.

These fringes are caused by the interferometer modulation of the radiation from the FOV. They are vertically oriented because for any interferometer angular position, the OPD between the two interferometer arms varies only in the horizontal direction: therefore, radiation from pixels on the same vertical column undergoes the same OPD. The central bright fringe is on the "zero OPD" pixels, at which all wavelengths interfere constructively. To the left of those pixels the OPD is of opposite sign as to the right of them. As the interferometer is scanned by rotation, the FOV remains stationary on the computer screen, and the fringes move with respect to the FOV to the right or to the left, depending on the direction of the interferometer scan. As mentioned above, after a complete rotational scan, all the interferograms are stored for all the pixels and all the spectra are now calculated by Fourier Transform.

Alternatively, the same interferogram information for the pixels of the FOV can be obtained if the interferometer is kept fixed and the optical head is rotated around a vertical axis (say for example by rotating the head of the tripod of figure 2 at constant speed), and the CCD frames are acquired as before. As the optical head is rotated, now the scene of the FOV moves horizontally, and the fringes remain stationary; after the head is rotated a large enough angle, the gathered information is the same. Figure 4 shows two CCD acquired images at two different optical head positions.

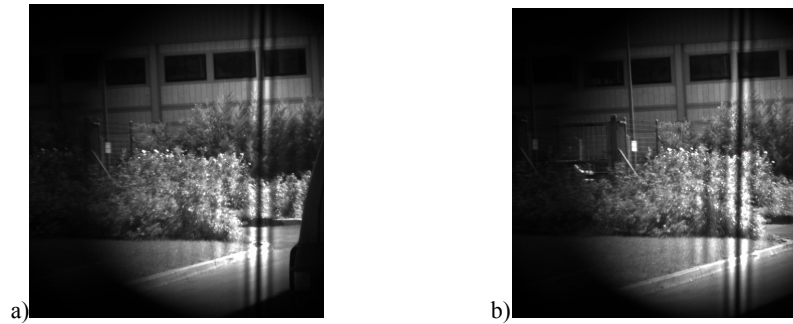


Figure 4: Two CCD acquired images for two optical head angular positions, while the interferometer is stationary in the optical head. The image moves horizontally, while the fringes remain stationary. The optical head rotation is equivalent to the aircraft movement, for the purposes of this explanation.

3. THE IR PUSHBROOM CONFIGURATION (SI 5000)

As explained in reference 4, a spectral imager as in figure 1 can be classified as an "Interferometric" "Framing" type, in which the scene to be observed has the same length as the width of the field of view of the instrument. Therefore, in this case, it is also a "staring" type. See Table 1 of reference 4 for the complete set of different types of spectral imagers.

The instrument as used in figure 4 belongs instead to the "Interferometric" "Windowing" classification of reference 4 and is a pushbroom configuration.

Suppose now that a fixed interferometer pushbroom type instrument is mounted down-looking in an aircraft, and aligned in such a way that the fringes on the image of the FOV are perpendicular to the travel direction of the aircraft. This is a situation similar to the one described in figure 4, the only differences being that the FOV is now to nadir instead of in a nearly horizontal direction and the length of the measured area on the earth surface is limited only by the distance traveled by the aircraft. So, such type of instrument used in this way belongs to the "Interferometric" "Windowing" class of reference 4, like the one described in figure 4.

3.1. Instrument modes of use

In summary, there are two basic modes of use for a fixed interferometer pushbroom type instrument using a shearing type interferometer like or similar to the one of figure 3 of reference 10: i) scanning the horizon by rotating the optical head around a nearly vertical direction, and ii) scanning a strip of earth surface by translating the optical head along with the aircraft in the flight direction.

Figure 5 shows the optical head mounted on a tripod for horizon scanning designed for 3 to 5 μ operation. Combined with a PC, special software and a stage controller, the system is called SI 5000.

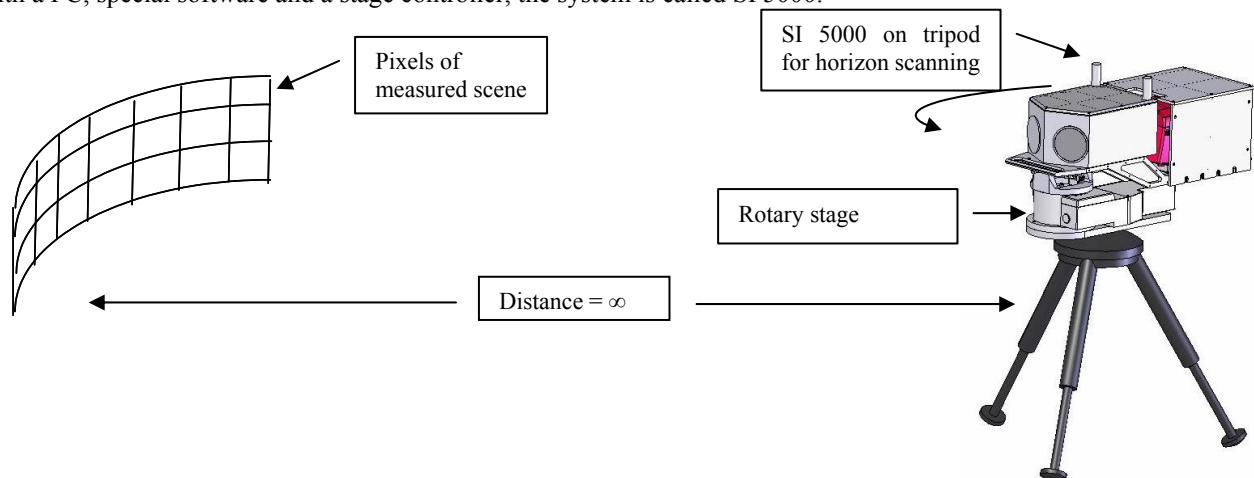


Figure 5: The SI 5000 is mounted on a horizontally rotating stage on a sturdy tripod. The instrument measures the IR self emission of each pixel of a horizon strip as function of wavelength, in a pushbroom configuration in the range 3 to 5 μ . Vertical field is 6.9° and horizontal field is up to 300° . The computer, stage controller and cables are not shown.

In this mode the instrument is controlled and operated by a PC and special software package with a rotation stage and stage controller for precise Field of View (FOV) scanning. The user first selects in the software the limits of FOV to be

scanned in the horizontal direction (for an FOV width up to 300° selected for convenience reasons) and then gives a "Start measurement" command by the click of a button. The SI 5000 then captures a sequence of IR frames at precise angular intervals in synchronization with the stage movement until the whole defined FOV is scanned. These frames carry all the information which will be sorted out by the software to construct the interferograms of each pixel of the selected FOV. These interferograms are then Fourier transformed and calibrated (using a previously measured blackbody spectrum at known temperature) to yield each pixel's intensity spectrum as function of wavelength in units of radiance. Additional software packages such as ENVI by ESRI and ITT can also be used with the system to implement further useful analysis, such as display of grey level images at different wavelengths, false color mapping according to spectral classification, statistical calculations on regions of interest, etc.

In the airborne mode the scanning for data collection is provided by the flight of the aircraft. As a result the stage is not used but positioning instrumentation (GPS) and position correction software is provided to compensate for the effects of random aircraft movement.

3.2. General optical design considerations

The two SI 5000 optical subsystems are i) the interferometer and ii) the collection optics. In this case reduction of total optics size is important for convenience of use, but also because it has a significant impact on overall cost, due to the high cost of IR suitable materials. As a consequence we devoted a significant effort to reducing the optics size as much as possible. The result of this effort is an innovative interferometer shape with internal beamsplitter as shown in figure 6. The higher index of refraction of the prism with respect to air further reduces the beam wander inside the interferometer at different FOV angles. The second result is a compact collection optics designed to image the system entrance pupil onto the cold shield plane of the nitrogen Stirling cooled FPA, so as to reduce background light as much as possible. Figure 7 shows the optical diagram of the SI 5000 including prism and collection optics. The same concept can be used for the 3 to 5 μ wavelength range as well as for the 8 to 12 μ range.

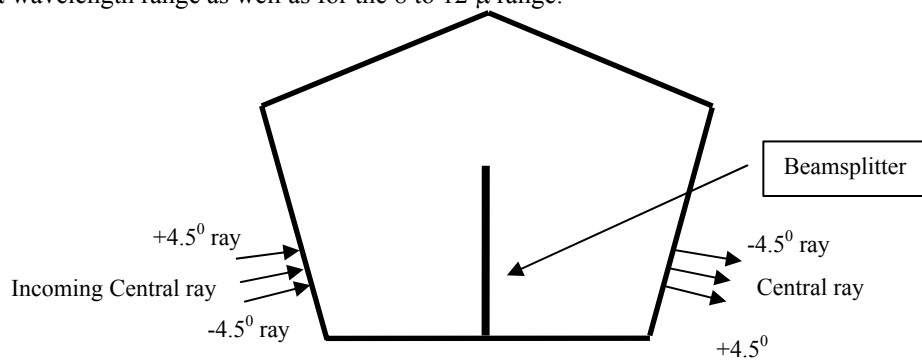


Figure 6: Interferometer prism: the beamsplitter surface is internal to the prism.

3.3. Optical layout

Figure 7 is the optical layout of the instrument.

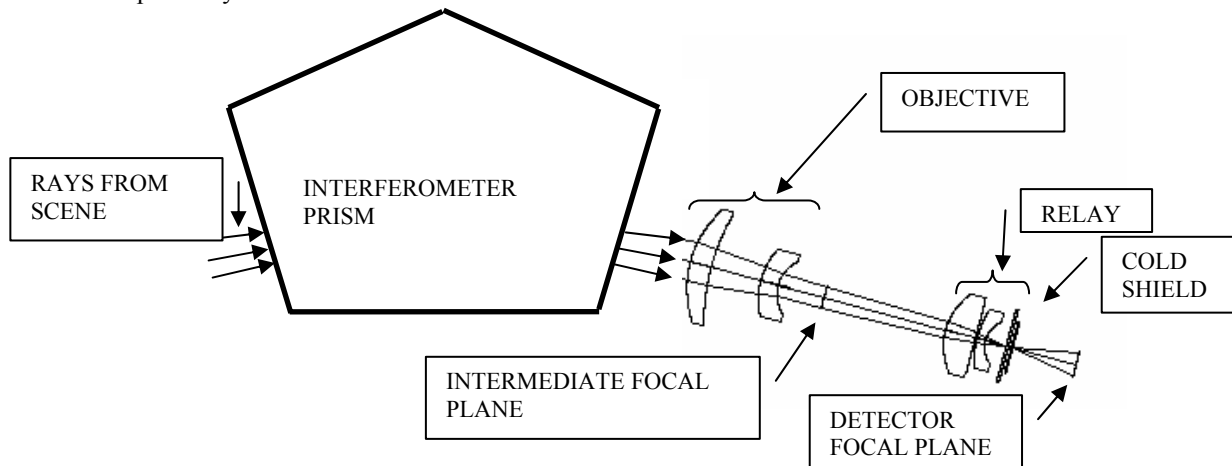


Figure 7: Optical layout of the SI 5000.

3.4. Expected performance

The design of prism beamsplitter and AR coatings, prism material and surface quality, optics MTF and focal length combined with the selected camera number of pixels and pixel size, pixel well fill capacity and other camera performance is expected to give the following system performance in the 3-5 μ range:

PARAMETER	VALUE
IFOV	0.5 milliradians
Spectral range	3 to 5 μ
Spectral resolution	50 cm^{-1} or better
Number of pixels	320x240
Noise Equivalent Spectral Radiance	2.5 x 10 ⁻⁹ Watt/(cm ² .sr .cm ⁻¹), at 4.8 microns and uniform blackbody source at 25C over the field of view.
Data acquisition time for 9.1x6.9 ⁰ FOV	~5 seconds
Working environment temperature	-10 to 40 C in the shade and no precipitation

The two most important characteristics of the optical design are the beamsplitter spectral transmission/reflection (TR) curves of the p and s polarization directions and the MTF curve of the collection optics versus spatial frequency. The requirement on the former is that the TR curves should be close to 50% for all wavelengths in the range at both p and s polarization directions. This insures that the measured spectrum will be nearly independent of any possible polarization of any scene pixel. The requirement on the latter is that the polychromatic MTF should be as close as possible to diffraction limit up to 17 cy/mm (which is 1/2 of the camera pixel spatial frequency 1/(30 μ) or spatial Nyquist frequency), with rms wavefront error less than 0.1 at all wavelengths and optimized for smallest distortion at the FOV sides. The MTF and rms wavefront error requirements insure high fringe visibility at all wavelengths, and of course good image quality.

Figure 8 shows the spectral transmittance curves for p and s directions for different angles in the FOV.

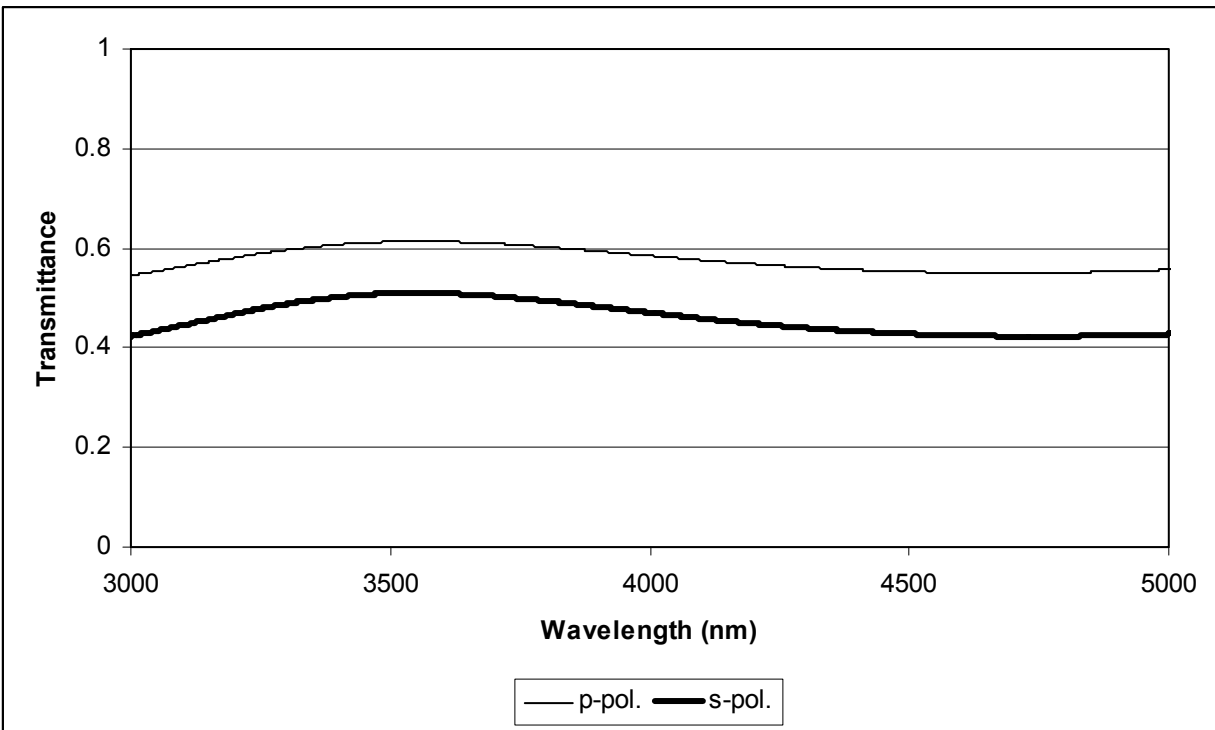


Figure 8: Transmittance curves for the p and s polarization directions of the central ray incident on the beamsplitter. All curves are between 40 and 60%. The reflectance curves are complementary to the transmittance curves since the beamsplitter absorptance is 0.

Figure 9 shows the polychromatic MTF curve in the range of interest.

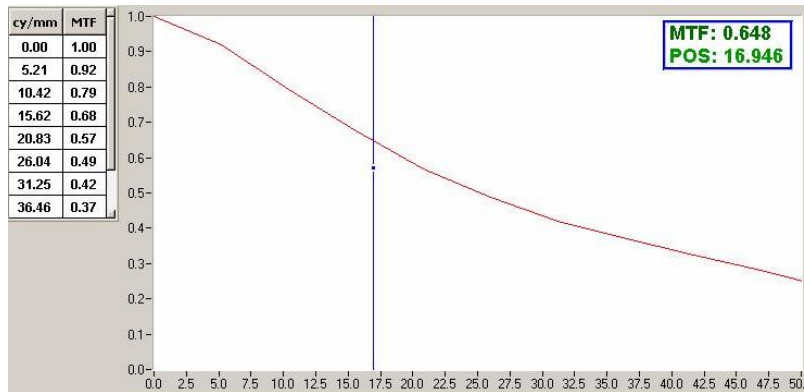


Figure 9: The as measured on-axis polychromatic MTF as function of spatial frequency in cycles/mm. on the focal plane of the collecting optics. Due to the 30 μ pixel size of the Focal Plane Array, the spatial Nyquist frequency is 17 cy/mm.

3.5. Calibration in spectral radiance units

The SI 5000 is a spectral imager, sensitive in the spectral region of 3-5 μ , whose output is a spectral radiance function for every pixel of the scanned region of space. The scan is done in a pushbroom fashion either by rotating or translating the optical head of the system. This radiance function is displayed in units of Watt/(sr.cm². μ ⁻¹). During the pushbroom scan an intensity function in units of volts is acquired for every pixel as function of the OPD (optical path difference) so that the radiation from that pixel goes through the interferometer. This function is then transformed into the calibrated spectrum by a mathematical algorithm. The system is optically aligned in such a way that one side of the detector array corresponds to the zero OPD region while the other side corresponds to the OPD_{max} region of the interferogram.

The purpose of this document is to describe the specific mathematical algorithm which transforms the intensity curve collected in volts for each pixel of the cube into its spectrum, calibrated in units of Watt/(sr.cm². μ ⁻¹).

3.5.1. The Physics

A fundamental assumption in this type of calibrated measurements is that the detector is “linear”. This means that the voltage output of each element of the array (the raw data) is linear with the well fill, which in turn is linear with the frame integration time for constant flux and with respect to flux for constant integration time. The detector manufacturer quotes linearity figures of the order of 0.01%, or one part per 10,000 after a standard NUC (non-uniformity correction) algorithm is applied to the measured volt values. From now on we will refer only to the raw data after NUC.

This linearity assumption allows us to label the instrument output with the radiance units Watt/(sr.cm². μ ⁻¹) by comparing the measurement of an unknown object with the measurement of a blackbody at one single known temperature.

However, there is an additional complication: self-emission of the optics and reflection by the optics of the internal wall of the lens holders is present and significant in the infrared region. Neither of the optics nor the optics mechanical holders is cooled; therefore this radiation reaches the detector and must be taken into account.

We first write the general relations between the signal, the detector response, the object radiance to be measured and this unwanted background radiation. Then we calculate and subtract from the signal the contribution of this background radiation. Finally, we measure a blackbody at known temperature and calculate the object radiance by comparison between the two measurements.

3.5.2. The Algorithm

The equations below refer to one single pixel, a representative of all the pixels of the image. The pixel is assumed to be filled with uniform radiance. As the pixel moves across the array elements, the system response may change somewhat. For simplicity we assume that this response remains constant.

Definitions:

Symbol	Parameter	Units
λ	Wavelength in the 3 to 5 micron region.	Microns (μ)
σ	Wavenumber $1/\lambda$	Inverse microns (μ^{-1})
$W(\sigma)$	Spectral radiance of an unknown object to be measured	Watt/(sr.cm ² . μ^{-1})
x	Optical Path Difference through the interferometer	Microns (μ)
$S(x)$	Interferogram of an unknown object	Volts

	as measured, including the effects of the spectral response of the detector, transmittance of the optics and the background discussed above	
I(x)	Ideal interferogram of an unknown object (assuming constant response function with wavelength, 100% transmittance of the optics and no self emission and reflection from the optics)	W/(sr.cm ²)
K(σ)	Spectral response of a detector array element (assumed to be the same for all the elements, since the volt values are after NUC) and including transmittance of the optics	Volt/[Watt/(sr.cm ² . μ ⁻¹)]
T	Calibration blackbody temperature	Kelvin
T _{room}	Room temperature	Kelvin
T _o	Optics temperature	Kelvin
P(T,σ)	Planck function at temperature T	Watt/(sr.cm ² . μ ⁻¹)

The ideal interferogram of an object whose collimated radiation traverses an interferometer with exactly 50-50% beamsplitter and 100% reflectance from the mirrors is:

$$I(x) = 1/2[I(0) + \int_{1/5\mu^{-1}}^{1/3\mu^{-1}} W(\sigma) \cos(2\pi\sigma x) d\sigma] \quad (1)$$

where

$$I(0) = \int_{1/5\mu^{-1}}^{1/3\mu^{-1}} W(\sigma) d\sigma \quad (2)$$

is the central burst value of the interferogram.

Since the instrument optics has a wavelength dependent transmittance and the detector has a wavelength dependent response function, we define two different functions K(σ) and K'(σ) expressing both effects, such that the actually measured signal from the pixel as function of OPD is as follows:

$$S(x) = 1/2 \left[\int_{1/5\mu^{-1}}^{1/3\mu^{-1}} K(\sigma) W(\sigma) d\sigma + \int_{1/5\mu^{-1}}^{1/3\mu^{-1}} K(\sigma) W(\sigma) \cos(2\pi\sigma x) d\sigma \right] + \int_{1/5\mu^{-1}}^{1/3\mu^{-1}} K'(\sigma) P(T_o, \sigma) d\sigma \quad (3)$$

Obviously, K and K' are different because the two optical paths are different. T_o is assumed to be the same as T_{room} and for now are both assumed to be constant in time during a measurement and also between a calibration and a measurement. Later we will see how to take into account a changing room temperature.

Now we note that the second term on the right side of equation (3) does not depend on x, because it does not go through the interferometer. In principle, the self-emission of the window of the instrument does go through the interferometer but it is a thin plate of very low emissivity material so that its self-emission contributes negligibly to the total signal. So we can replace the second term on the right side of equation (3) with a constant A. From (3), setting x=0:

$$S(0) = \int_{1/5\mu^{-1}}^{1/3\mu^{-1}} K(\sigma) W(\sigma) d\sigma + A \quad (4)$$

So, by multiplying (3) by 2 and taking into account (4):

$$\begin{aligned}
2S(x) &= \int_{1/5\mu^{-1}}^{1/3\mu^{-1}} K(\sigma)W(\sigma)d\sigma + \int_{1/5\mu^{-1}}^{1/3\mu^{-1}} K(\sigma)W(\sigma)\cos(2\pi\alpha x)d\sigma + 2A = \\
&= S(0) + \int_{1/5\mu^{-1}}^{1/3\mu^{-1}} K(\sigma)W(\sigma)\cos(2\pi\alpha x)d\sigma + A
\end{aligned} \tag{5}$$

Subtracting $S(0)+A$ from (5), Fourier transforming both sides, and dividing by $K(\sigma)$ we can express the final result for $W(\sigma)$ as follows:

$$W(\sigma) = \frac{1}{K(\sigma)} F[2S(x) - S(0) - A] \tag{6}$$

Now we note that the spectrum to be measured is usually a wide spectrum and that $K(\sigma)$ is a smooth function of σ ; as a result we can assume that on the high OPD side of the array the OPD is large enough for the second term in square parenthesis of equation (3) to vanish. This happens for OPD values (x) far enough from the central burst. This is not a very restrictive assumption because this background is approximately the same for all the pixels; as a consequence we can use for A the same value found for any pixel whose spectrum is wide enough and for which the second term in the square parenthesis of (3) vanishes. So we have:

$$S(\infty) = \frac{1}{2} \int_{1/5\mu^{-1}}^{1/3\mu^{-1}} K(\sigma)W(\sigma)d\sigma + A \tag{7}$$

The symbol ∞ stands for an OPD near OPD_{\max} . Solving for $\int_{1/5\mu^{-1}}^{1/3\mu^{-1}} K(\sigma)W(\sigma)d\sigma$ from (7) and substituting it into (4), we

get:

$$S(0) = 2S(\infty) - 2A + A = 2S(\infty) - A \tag{8}$$

or

$$A = 2S(\infty) - S(0) \tag{9}$$

Substituting (9) into (6) we get:

$$W(\sigma) = \frac{2}{K(\sigma)} F[S(x) - S(\infty)] \tag{10}$$

In equation (10) $S(x)$ and $S(\infty)$ are measured, so in order to find $W(\sigma)$ we still have to find $K(\sigma)$. This will be done by measuring an external blackbody at known temperature T , as follows.

The corresponding signal function $S_C(x)$ in equation (3) with $P(T,\sigma)$ instead of $W(\sigma)$, similarly to (10), gives:

$$K(\sigma)P(T,\sigma) = 2F[S_C(x) - S_C(\infty)] \tag{11}$$

Finally, we have, by dividing (11) by $P(T,\sigma)$:

$$K(\sigma) = \frac{2F[S_C(x) - S_C(\infty)]}{P(T,\sigma)} \tag{12}$$

To find $W(\sigma)$ from equation (10) we now substitute $K(\sigma)$ from (12) into (10):

$$W(\sigma) = \frac{F[S(x) - S(\infty)]}{F[S_C(x) - S_C(\infty)]} P(T,\sigma) \tag{13}$$

All the quantities on the right side of (13) are known, and so $W(\sigma)$ can be calculated. The result is in the desired units of $\text{Watt}/(\text{sr}\cdot\text{cm}^2\cdot\mu^{-1})$ because the fraction on the right side of (13) is unitless, and $P(T,\sigma)$ is expressed in those units.

3.5.3. Changing optics temperature

Changing optics temperature among measurements but not within a measurement

If the optics temperature changed between the calibration measurement and the measurement of the unknown object but it remained constant within the same measurement, then in general the A constant that we define for $S_c(x)$, A_c , is different than A:

$$A_c \neq A \quad (14)$$

However, (10), (11) and (12) are still valid, each with its own value of A, and therefore (13) is still valid too.

Changing optics temperature within a measurement

If the optics temperature changed during a measurement, the problem is clear from equation (9): A can be calculated only after the whole OPD scan has been made. As a result, the instantaneous value of A cannot be retrieved from (9).

In general, we expect that there is no point in measuring at slower frame rates than the maximum 180 Hz, because the maximum allowed integration time is 5 msec., so a slower frame rate would be a waste of time, and also would increase the chance that the object moves during the measurement. In these conditions, it follows that the optical head should not be scanned at slower angular speed than $1 \Delta\text{OPD} \cdot 180\text{Hz} = 90 \text{ milliradian/sec.} = 5.14^0/\text{sec.}$, since one ΔOPD corresponds to one pixel or half a milliradian. This is because otherwise the spectral cube measurement (a minimum of 640 frames for a full FPA field of view of 9.1^0) will take longer than 3.6 seconds. If better signal to noise is required, it is recommended to repeat the measurement of the same image several times and average the resulting cubes.

From what is said above we can calculate the slowest frequency of the information carrying signals in the interferogram of a pixel. This is found as follows.

First we note that since there is no signal outside the 3 to 5 microns wavelength range, and the optics is aligned for two pixels per fringe at 3 microns, there is no information at slower spatial frequency than $(5/3 \times 2 \Delta\text{OPD})^{-1}$ corresponding to $(5/3 \times 1 \text{ milliradian})^{-1} = (1.7 \text{ mrad})^{-1}$ or $(3.4 \text{ pixels})^{-1}$ frequency. This is scanned in a time = $1.7/90 \text{ sec.} = 19 \text{ millisecond}$. The corresponding time frequency is 53 Hz. This means that if we filter the interferogram with a spatial high pass filter with cut-on at slightly less than 0.29 pixel^{-1} or $0.29 \Delta\text{OPD}^{-1}$ there is no loss of information.

This spatial cut-on operator performs two functions at once:

- a. It subtracts the $S(\infty)$ term of equations (10) and (11) above which is a DC term, and
- b. It subtracts any optics self-emission and reflection drifts due to temperature changes at characteristic frequencies lower than 53 Hz or time changes of characteristic times longer than 19 milliseconds.

4. CONCLUSION

In this paper we describe a new 3 to 5 μ spectral imager, the SI 5000. We showed how an interferometric design can be used for spectral imaging in a pushbroom horizon or airborne earth surface scanning configuration. The most important characteristics are: no optics cooling and convenient system operation in a commercially available package. We also showed here how the instrument is calibrated in radiance units of $\text{Watts}/(\text{cm}^2 \cdot \text{sr} \cdot \mu)$ or $\text{Watts}/(\text{cm}^2 \cdot \text{sr} \cdot \text{cm}^{-1})$.

In a future paper, as we gather more experience with the system, we will give further measured results on its performance and applications examples.

ACKNOWLEDGMENTS

The authors wish to thank Mr. Ziv Attar for the design of the collection optics to CI Systems specifications and for useful discussions. They also wish to thank Mr. Henry Orr of NDC Infrared Engineering Ltd. for discussions and help with the interferometer coating design and implementation to CI Systems specifications.

REFERENCES

1. Dario Cabib et al., New airborne pushbroom spectral imager for the 3-5 and 7-12 μ wavelength ranges, Conference Proceedings of the XXXI Symposium of the Optical Society of India, ICOL-2005, Dehradun, India, December 12-15, 2005.
2. Paul G. Lucey et al., High-performance Sagnac interferometer using uncooled detectors for infrared hyperspectral applications, SPIE Proc. Vol. 6565, 2007.
3. Paul G. Lucey et al., High-performance Sagnac interferometer using cooled detectors for infrared LWIR hyperspectral imaging, SPIE Proc. Vol. 6546, 2007.
4. R.G. Sellar and G.D. Boreman, Classification of imaging spectrometers for remote sensing applications, Optical Engineering Vol. 44(1), 2005, p. 013602-1.
5. J.F. Harrison et al., Earth-Observing Hyperspectral Imaging Systems: A 2003 Survey, SPIE Proc., Vol.5097, 2003, p. 222.
6. Nahum Gat et al., Spectral Imaging Applications: Remote Sensing, ..., SPIE Proc., Vol. 2962, 1997, p.63.
7. R.F. Horton, Optical design for a high-étendue imaging Fourier-transform spectrometer, SPIE Proc., Vol. 2819, 1996, p. 300.

8. Schrock, E., et al., Multicolor spectral karyotyping of human chromosomes. *Science*, 1996. 273(5274): p. 494-7.
9. R.A. Keller and T.S. Lomheim, Imaging Fourier Transform Spectrometer (IFTS): Parametric Sensitivity Analysis, *SPIE Proc.*, Vol. 5806, paper no. 5806-29, 2005.
10. Dario Cabib et al., Spatially resolved Fourier Transform spectroscopy (Spectral Imaging): a powerful tool for quantitative analytical microscopy, *SPIE Proc.*, Vol. 2678, 1996, p. 278.